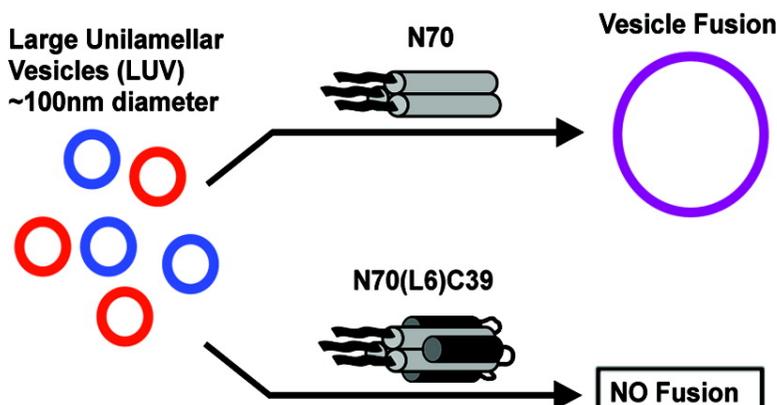Article

Hairpin Folding of HIV gp41 Abrogates Lipid Mixing Function at Physiologic pH and Inhibits Lipid Mixing by Exposed gp41 Constructs

Kelly Sackett, Matthew J. Nethercott, Yechiel Shai, and David P. Weliky

More About This Article

Additional resources and features associated with this article are available within the HTML version:

- Supporting Information
- Access to high resolution figures
- Links to articles and content related to this article
- Copyright permission to reproduce figures and/or text from this article

View the Full Text HTML

ACS Publications
High quality. High impact.

Hairpin Folding of HIV gp41 Abrogates Lipid Mixing Function at Physiologic pH and Inhibits Lipid Mixing by Exposed gp41 Constructs[†]

Kelly Sackett,[‡] Matthew J. Nethercott,[‡] Yechiel Shai,[§] and David P. Weliky*,[‡]

Department of Chemistry, Michigan State University, East Lansing, Michigan 48824, and Department of Biological Chemistry, Weizmann Institute of Science, Rehovot 76100, Israel

Received October 17, 2008; Revised Manuscript Received February 12, 2009

ABSTRACT: Conformational changes in the HIV gp41 protein are directly correlated with fusion between the HIV and target cell plasma membranes, which is the initial step of infection. Key gp41 fusion conformations include an early extended conformation termed prehairpin which contains exposed regions and a final low-energy conformation termed hairpin which has a compact six-helix bundle structure. Current fusion models debate the roles of hairpin and prehairpin conformations in the process of membrane merger. In the present work, gp41 constructs have been engineered which correspond to fusion relevant parts of both prehairpin and hairpin conformations and have been analyzed for their ability to induce lipid mixing between membrane vesicles. The data correlate membrane fusion function with the prehairpin conformation and suggest that one of the roles of the final hairpin conformation is sequestration of membrane-perturbing gp41 regions with consequent loss of the membrane disruption induced earlier by the prehairpin structure. To our knowledge, this is the first biophysical study to delineate the membrane fusion potential of gp41 constructs modeling key fusion conformations.

HIV initiates infection of target cells through a process of fusion between the viral envelope membrane and the cell plasma membrane at physiologic pH. The viral transmembrane (TM)[1] protein gp41 catalyzes this process through direct interaction with the target cell membrane and through conformational changes (see Figure 1) (*1, 2*). gp41 is one of two subunits of the envelope (ENV) complex and is initially shrouded by the gp120 subunit on the virion surface (Figure 1A). The putative oligomerization state of ENV is a trimer with three gp41 and three gp120 subunits (*3*). Activation of gp41 is triggered by sequential binding of gp120 to cell surface CD4 receptor (*4*) and coreceptor (*5*) which induces gp120 conformational changes. These changes allow the gp41 region outside the virus (ectodomain) to adopt an extended conformation (*6, 7*) and anchor into the target cell membrane via its N-terminal apolar fusion peptide (FP)

region (*8, 9*). This early exposed gp41 conformation is termed the prehairpin intermediate (PHI) (Figure 1B). At a later time in the fusion process, gp41 folds into a lower energy final-state hairpin conformation (Figure 1C) (*10*).

The gp41 ectodomain is comprised of FP, N-terminal heptad repeat (NHR), disulfide loop, C-terminal heptad repeat (CHR), and membrane proximal external region (MPER) (Figures 1B and 2A). Development of fusion models has relied on high-resolution structures of gp41 constructs in the hairpin conformation. These structures reveal compact six-helix bundle (SHB) assembly of NHR and CHR regions whereby trimeric parallel coiled-coil NHR forms an internal core, and three CHR helices pack antiparallel into the hydrophobic coiled-coil grooves (Figures 1C and 2D) (*2, 11, 12*). No high-resolution data exist for FP, MPER, or loop regions of HIV gp41 in context of the folded SHB. The apolar FP region is essential to fusion because of its membrane insertion (*8, 9*) and oligomerization properties (*13*). A critical gp41 fusion conformation, the exposed PHI, is targeted by exogenous NHR or CHR fragments which bind counterpart regions in viral PHI to reproduce hetero-SHB organization with consequent inhibition of viral fusion in a dominant negative manner (*1*). Established clinical efficacy of a CHR-derived fusion inhibitor underscores the importance of understanding the correlation between gp41 conformation and viral fusion (*14*).

Predominant fusion models postulate that PHI to hairpin folding drives viral fusion by drawing viral and cell membranes into close proximity (*1, 2*). Alternatively, there is some evidence that the process of membrane fusion is carried out primarily by gp41 in an earlier conformation prior to the final folded hairpin, implying a more central fusion role for the exposed PHI (*10*). The specific roles of hairpin

* Address correspondence to this author. Phone: 517-355-9715. Fax: 517-353-1793. E-mail: weliky@chemistry.msu.edu.

‡ Michigan State University.

§ Weizmann Institute of Science.

[1] Abbreviations: CD, circular dichroism; chol, cholesterol; CHR, C-terminal heptad repeat; C-PHI, C-terminal half of the prehairpin intermediate. D-malt, *n*-decyl *β*-D-maltopyranoside; ENV, envelope; FP, fusion peptide; HEPES, *N*-(2-hydroxyethyl)piperazine-*N*′-2-ethanesulfonic acid; LUV, large unilamellar vesicle; MPER, membrane proximal external region; NCL, native chemical ligation; NHR, N-terminal heptad repeat; N-PHI, N-terminal half of the prehairpin intermediate; PHI, prehairpin intermediate; POPC, 1-palmitoyl-2-oleoyl-*sn*-glycero-3-phosphocholine; POPG, 1-palmitoyl-2-oleoyl-*sn*-glycero-3-[phospho-*rac*-(1-glycerol)]; RP-HPLC, reverse-phase high-performance liquid chromatography; SHB, six-helix bundle; SUV, small unilamellar vesicle; TCEP, tris(2-carboxyethyl)phosphine hydrochloride; TM, transmembrane.
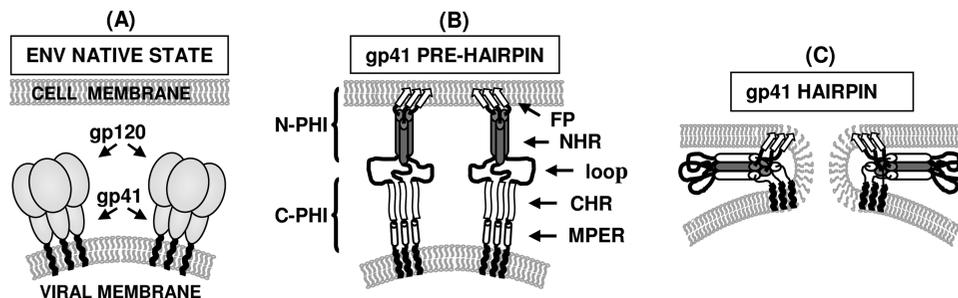
FIGURE 1: (A−C) HIV fusion model. (B, C) gp120 is not shown in order to focus on gp41 organization. The FP region is indicated using arrows.

and PHI conformations toward gp41-directed membrane fusion are not clear. Comparative analysis of gp41 constructs modeling hairpin and PHI fusion conformations in model membrane fusion systems can help to elucidate their *in vivo* fusion roles.

To understand which component and/or conformation of gp41 is involved in the actual steps of membrane merger, we analyzed the gp41 constructs termed FP34, N70, N47(L6)C39, and N70(L6)C39 (Figure 2) for global conformation and their ability to induce lipid mixing of large unilamellar vesicles (LUVs). FP34 represents the membrane-interacting N-terminal FP region of gp41. N70 is comprised of FP and NHR regions and reproduces the organization of the N-terminal half of the exposed PHI conformation (N-PHI) (*15*), which is a key drug target (Figures 1B and 2B). N47(L6)C39 models the folded hairpin conformation, with the wild-type loop between NHR and CHR regions replaced by a minimal six-residue loop (L6) (Figure 2D), which does not affect SHB assembly (*12*). N70(L6)C39 is identical to N47(L6)C39 but is extended N-terminally to include the FP and models the folded hairpin in context of the FP (Figure 2C). The results of this paper show that exposed regions of gp41 are primarily responsible for the steps of membrane merger. Folded gp41 SHB, with or without the FP region and lacking the native loop, is nonfusogenic at physiologic pH and inhibits fusion directed by exposed gp41 constructs (FP34 and N70). Our results are discussed in context of gp41-mediated HIV fusion.

EXPERIMENTAL PROCEDURES

Materials. Boc and Fmoc amino acids, Boc MBHA resin, and Fmoc rink amide MBHA resin were purchased from Novabiochem. *S*-Trityl-*β*-mercaptopropionic acid was purchased from Peptides International (Louisville, KY). Other reagents for peptide synthesis, TCEP (tris(2-carboxyethyl)phosphine hydrochloride), *N*-(2-hydroxyethyl)piperazine-*N′*-2-ethanesulfonic acid (HEPES), and Triton X-100, were purchased from Sigma. *N*-(7-Nitro-2,1,3-benzoxadiazol-4-yl)phosphatidylethanolamine (*N*-NBD-PE), *N*-(lissamine rhodamine B sulfonyl)phosphatidylethanolamine (*N*-Rh-PE), 1-palmitoyl-2-oleoyl-*sn*-glycero-3-phosphocholine (POPC), 1-palmitoyl-2-oleoyl-*sn*-glycero-3-[phospho-*rac*-(1-glycerol)] (POPG), *n*-decyl *β*-D-maltopyranoside (D-malt), and cholesterol were purchased from Avanti Polar Lipids, Inc. (Alabaster, AL). The micro bicinchoninic acid protein assay was obtained from Pierce (Rockford, IL). All other reagents were of analytical grade.

Peptide Synthesis. Synthetic peptide sequences are based on the HXB2 strain of HIV-1 ENV as follows: (a)
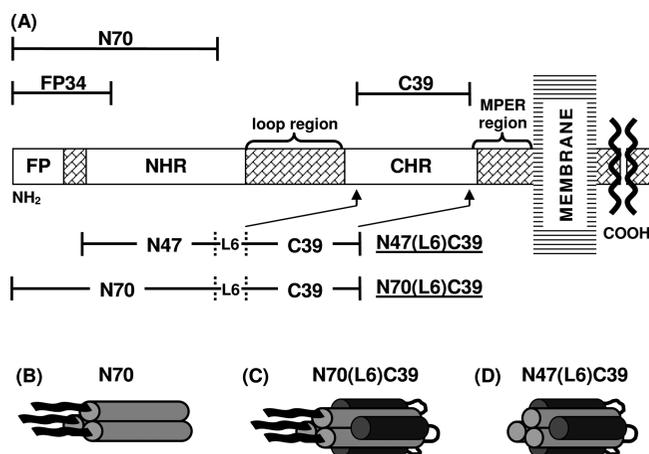

FIGURE 2: (A) Schematic of the HIV-1 gp41 ectodomain. Primary functional regions are designated by white boxes, and additional functional regions are specified above in braces. Above and below in brackets are the gp41 fragments under study. (B−D) Structural representation of N70 and structural models of N70(L6)C39 and N47(L6)C39, respectively.

FP34(linker) 512−545-(thioester), (b) FP23(linker) 512−534-(S534A)-(thioester), (c) FP34 512−545, and (d) N36(S546C) 546−581. FP34(linker) and N36(S546C), both used in the preparation of N70, as well as FP34 and FP23(linker) were prepared as described previously (*15, 16*). Synthetic peptides were purified to ∼95% purity by reverse-phase high-performance liquid chromatography (RP-HPLC) on C18 or C4 semipreparative columns using a linear gradient between water/0.1% trifluoroacetic acid (TFA) and 10% water/90% acetonitrile/0.1% TFA. Purified peptides were lyophilized and stored at −20 °C under argon. Peptide quantification to an accuracy of ±6% was carried out using a bicinchoninic acid assay. Mass spectroscopy was used to confirm the mass of each purified peptide.

Protein Expression. The HIV-1 HXB2 strain ENV insert in a pAED4 plasmid was the template for engineering N47(L6)C39 DNA. Primers were designed to individually transcribe NHR (residues 535(M535C) to 581) and CHR (residues 628 to 666) segments, including codons for the SGGRGG minimal loop residues both on the C-terminal peptide end of the NHR and on the N-terminal peptide end of the CHR fragments as well as start and stop codons. Following PCR amplification and purification of NHR and CHR gene fragments, the two were hybridized through their common SGGRGG loop bases, and the N47(L6)C39 coding sequence was then amplified by PCR and purified. The N47(L6)C39 coding sequence was hybridized to a fragment from pET11a which includes T7 promoter and ribosome binding site, and this PCR-amplified and purified sequence

was ligated into a pGEMt vector and transformed into BL-21 *Escherichia coli* cells. N47(L6)C39 was designed to be a minimal construct with SHB or equivalently hairpin structure lacking the FP region and with the native loop replaced by a minimal SGGRGG loop (Figure 2D). The lengths of NHR and CHR regions were selected considering both SHB stability and native chemical ligation (NCL) reaction requirements as follows: (a) Wild-type methionine at the N-terminus is mutated to cysteine (M535C) for the purpose of NCL. (b) The C-terminus of the NHR fragment and the N-terminus of the CHR fragment were selected to be complementary based on a crystal structure (*11*). (c) Assuming fully helical NHR and CHR fragments in folded SHB assembly, the C-terminus of the CHR region was selected to complement the NHR fragment while leaving 2−3 residues at the N-terminus of the NHR fragment conformationally free to facilitate NCL at the N-terminal cysteine residue. Expression was done in BL-21 cells using the T7 expression system. Following bacteria growth, IPTG induction, and growth, the centrifuged cell pellet was lysed with glacial acetic acid. The supernatant was diluted to 10% acetic acid, filtered, and concentrated; then the N47(L6)C39 fragment was purified to ∼95% homogeneity by RP-HPLC using a C18 preparative column and a multistep gradient, followed by lyophilization and storage under argon at −20 °C. Mass spectroscopy confirmed the purified protein mass, and quantification was based on UV absorption at 280 nm.

Native Chemical Ligation. N70 was prepared by ligating FP34(linker) with N36(S546C) as described previously (*15*). The construct N70(L6)C39 was prepared in an identical manner by ligating FP23(linker) with N47(L6)C39, and it was designed to model the folded hairpin including the N-terminal FP region (Figure 2C). Ligation reactions were purified by RP-HPLC using a C4 semipreparative column and a linear gradient, with ligation product N70 or N70(L6)C39 eluting as a single isolated peak whose mass was confirmed by mass spectroscopy. N70(L6)C39 was refolded by dialysis into 10 or 20 mM formate buffer at pH 3.0 with 200 μM TCEP and stored at 4 °C, while N70 was lyophilized and stored under argon at −20 °C. Quantification was based on the bicinchoninic acid assay (N70) or UV absorption at 280 nm (N70(L6)C39).

Lipid Preparation. POPC:POPG:chol (8:2:5 molar ratio) LUVs with ∼100 nm diameter were prepared through extrusion as described previously in a 25 mM HEPES, pH 7.5, buffer and with total POPC + POPG + chol concentration of 225 μM (*17*). This composition reflects (a) choline being the dominant headgroup of membranes of host cells of HIV and (b) the cholesterol and negatively charged headgroup content of these membranes (*18*).

Lipid-Mixing Assay of Membrane Fusion. A fluorescence assay was used to probe gp41 construct-induced intervesicle lipid mixing, which is one feature of vesicle fusion (*19*). The protocol for the assay has been previously described (*20*). A Fluorolog-2 fluorometer was used to follow fluorescence changes in 1.2 mL LUVs under constant stirring at 37 °C following addition of 7−130 μL aliquots of peptide/protein solution. Peptide and protein samples were purified by HPLC and were either lyophilized or dialyzed extensively (minimal 10000:1 dilution) to remove acetonitrile that may affect the lipid mixing assay. The samples were of high purity (approximately 95%) based on both HPLC and

electrospray mass spectroscopy analysis. Peptide/protein solutions were prepared with either (a) 40 μM peptide or protein in "buffer" that contained 10 mM formate and 200 μM TCEP at pH 3.0 or (b) 80 μM peptide or protein in "detergent" that contained 10 mM formate, 0.5% D-malt, and 200 μM TCEP at pH 3.0. Low pH was required to maintain solubility of N70(L6)C39. An aliquot of the protein solution was added to the LUV solution, and the final pH was 7.2−7.3 with maximal protein concentration of 4 μM. A small fraction of the LUVs was "labeled" with fluorescent and quenching lipids, and protein-induced fusion with unlabeled vesicles resulted in increased fluorophore−quencher distances and higher fluorescence. After addition of protein, the time-resolved change in fluorescence, $\Delta F(t)$, was measured, and then 12 μL of 10% Triton X-100 was added to completely solubilize the lipids and cholesterol, creating maximal separation between fluorophore and quencher phospholipids. The consequent maximum fluorescence change, ΔF_{max}, was calculated as the difference between the fluorescence following addition of Triton and the initial LUV fluorescence (without protein). Small changes in fluorescence were observed upon addition of buffer or detergent alone to the LUV solution, and both $\Delta F(t)$ and ΔF_{max} were corrected for changes due to buffer or detergent alone. The "% lipid mixing" or $M(t)$ was calculated using $M(t) = \Delta F(t)/\Delta F_{max} \times 100$. All lipid mixing assays were repeated minimally in triplicate using different vesicle preparations and different batches of peptide and protein. For replicates using the same vesicle and protein or peptide preparations, the typical range of variation in the long-time value of $M(t)$ was ±2%. For different batches of the fusogenic peptide FP34, the maximum variation was ±8%, and for N70, the maximum variation was ±6%. These peptides always demonstrated a clear dose response, and the batch-to-batch variations may be due to differences in concentration of the hydrophobic peptides dissolved in aqueous solutions from lyophilized stocks.

Vesicle Enlargement. Protein-induced formation of larger vesicle bodies was qualitatively measured using transmission of visible radiation through the vesicle solution. Larger particles scatter more radiation and result in reduced absorbance. The assays were done with the same protein, lipid, and cholesterol concentrations and the same temperature as were used in the lipid mixing assays. A SpectraMax M2 microplate reader from Molecular Devices was used to measure the absorbance at 405 nm for a solution containing 200 μL of POPC:POPG:chol LUVs in 25 mM HEPES, pH 7.5, buffer. Aliquots of protein at 40 μM in buffer (22 μL) or at 80 μM in detergent (11 μL) were then added to the vesicle solution, and after 10 min incubation time, the absorbance at 405 nm was measured and the absorbance difference determined from subtraction of the vesicle-only value. All measurements were done in triplicate. For the FP34, N70, and N47(L6)C39 constructs, there was negligible change in absorbance at 405 nm when the protein was added to 25 mM HEPES, pH 7.5, buffer which did not contain LUVs.

Circular Dichroism (CD) Spectroscopy. Far-UV CD spectra were obtained at 37 °C using a 0.1 cm path length cuvette for solutions that contained 20 μM protein in "buffer", i.e., 20 mM formate and 200 μM TCEP at pH 3.0, or 20 μM protein in "detergent", i.e., 20 mM formate, 0.5%

D-malt, and 200 μM TCEP, pH 3.0. For near-UV spectra, protein concentrations were 40 μM in the same solutions, and spectra were recorded using a 1.0 cm path length cuvette at 25 °C. Spectra were recorded on a Chirascan CD spectrometer (Applied Photophysics Limited, Leatherhead, U.K.) with 1 nm increments and 5 s averaging time for far-UV spectra and with 0.5 nm increments and 2 s averaging time for near-UV spectra. The signal of buffer or detergent was subtracted from the sample signal. Triplicate measurements were averaged for far-UV spectra of FP34 and for near-UV spectra of N47(L6)C39 and N70(L6)C39 samples because of low signal. Following spectral acquisition, thermal melts were recorded at 222 nm with 5 °C steps and 1 °C/min ramp rate. The α-helical content was estimated from the CD signal at 222 nm with $\theta_{222} = -33000$ deg cm^2 dmol^{-1} correlating with 100% helicity (15).

RESULTS

The buffer pH was 3.0 rather than 7.4 to increase solubility of the FP-containing constructs and thereby attain the 40−80 μM stock protein concentration needed for the lipid mixing assay. All constructs were fully soluble at pH 3.0 as evidenced by transparent solutions and by no loss in protein concentration after centrifugation at 16000g. However, it is noted that, at pH 3.0, the FP region promotes formation of soluble aggregates of folded gp41 coiled coils and hairpin trimers (15). To assess the effects of such aggregation, studies were also carried out with initial protein solubilization in detergent that contained nondenaturing D-malt with the idea that detergent would reduce protein aggregation.

In addition, the bicinchoninic acid assay was used to analyze the solubilities of the constructs in the final conditions of the lipid mixing assay minus vesicles, i.e., nominal protein concentration of 4 μM and pH 7.2. N70, FP34, and N47(L6)C39 were fully soluble under these conditions as evidenced by transparent solutions and no reduction in protein concentration after centrifugation at 16000g. These results were independent of the presence or absence of D-malt in the solution. N70(L6)C39 exhibited partial precipitation, and the final concentration in the supernatant after centrifugation was 0.5−1.0 μM where the range reflects the results from four trials.

Figure 3 shows the kinetic lipid mixing traces following addition of gp41 constructs to POPC:POPG:chol vesicles. Extremely rapid lipid mixing is observed for N70 initially dissolved in either buffer or detergent (Figure 3A+B) and to a similar extent as previously reported for N70 predissolved in dimethyl sulfoxide (16). In buffer, N70 is in equilibrium between discrete trimers and aggregates of trimers, and the driving forces for the two types of self-association are the coiled-coil NHR and the nonhelical FP region, respectively (15). Detergent includes micellar nondenaturing D-malt for the purpose of dissolving peptide/protein aggregation without denaturing folded structure. Thus, higher order aggregates of N70 trimers observed previously in buffer (15) do not appear to significantly affect fusion function.

The characteristic time for N70-induced lipid mixing appears to be comparable to or shorter than the 3−5 s dead time of the assay. The lipid mixing rate of N70 is therefore at least as fast as that of a chemically cross-linked FP trimer
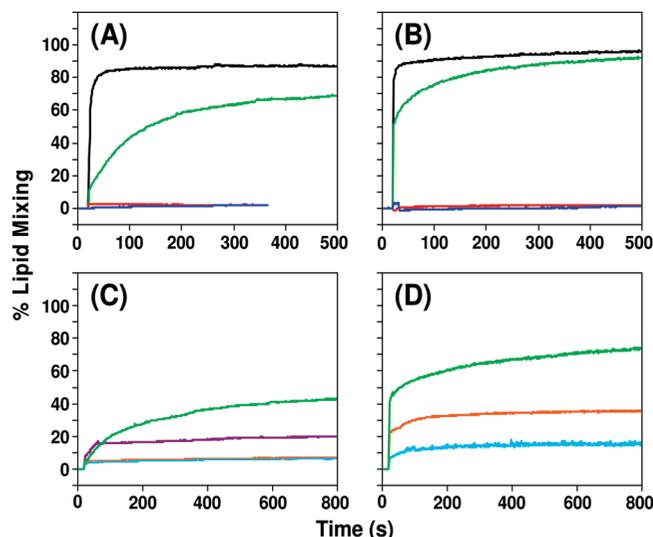

FIGURE 3: Lipid mixing of POPC:POPG:chol vesicles induced by gp41 constructs. At 20 s, gp41 constructs in buffer (A and C) or detergent (B and D) were added to vesicles with 150 μM total lipid and 75 μM cholesterol concentrations. For panels A and B, traces are as follows: 3.3 μM N70 (black), 3.3 μM FP34 (green), 4.0 μM N70(L6)C39 (blue), and 4.0 μM N47(L6)C39 (red). For panels C and D, traces are as follows: 2.25 μM FP34 (green), 2.25 μM FP34 with 1.5 μM N70(L6)C39 added at 70 s (purple), 2.25 μM FP34 with 1.5 μM N70(L6)C39 premixed (light blue), and 2.25 μM FP34 added following 5 min preincubation of vesicles with 1.5 μM N70(L6)C39 (orange).

(17), which supports a model that the most effective fusion is induced by small exposed FP oligomers (such as those formed by N70 or by cross-linked FPs) and less fusion is induced by large aggregates or monomers (17, 21). While the final extent of lipid mixing induced by N70 is comparable whether N70 is initially dissolved in buffer or detergent (Figure 3A,B), visual comparison of the two data sets suggests that the fusion rate may be somewhat faster in detergent. An effort was made to fit the N70 data to the sum of two exponential buildup functions, but it was not possible to accurately determine the rate of the fast component.

Figure 4 compares global secondary structure of gp41 constructs. N70 has significant α-helical content in buffer and detergent at 37 °C as evidenced by the shape of the CD spectra and the minima at 208 and 222 nm. This is consistent with previous analysis of N70 in buffer at 25 °C which revealed α-helical coiled-coil assembly in the NHR and nonhelical structure in the N-terminal FP region (15). Relative to buffer, more negative θ_{222} for N70 in detergent is consistent with additional α-helical structure ($\sim$14 residues; see Table 1). This finding correlates with the NMR structure of a discrete FP fragment in both zwitterionic and negatively charged micellar detergent which revealed α-helical FP conformation (22). N70 melts with a transition temperature of $\sim$45 °C in buffer, and stabilization of N70 coiled-coil structure by detergent (Figure 4A inset) correlates with α-helical structure promotion.

We attribute the slow fusion rate of FP34 in buffer (Figure 3A) to an initially unstructured form (Figure 4B) that may be aggregated since the FP region drives aggregation of otherwise monodisperse gp41 hairpins or trimeric NHR coiled coils at low pH (15). In this model, significant aggregation of FP34 in solution decreases the effective concentration of membrane-interacting and -perturbing pep-
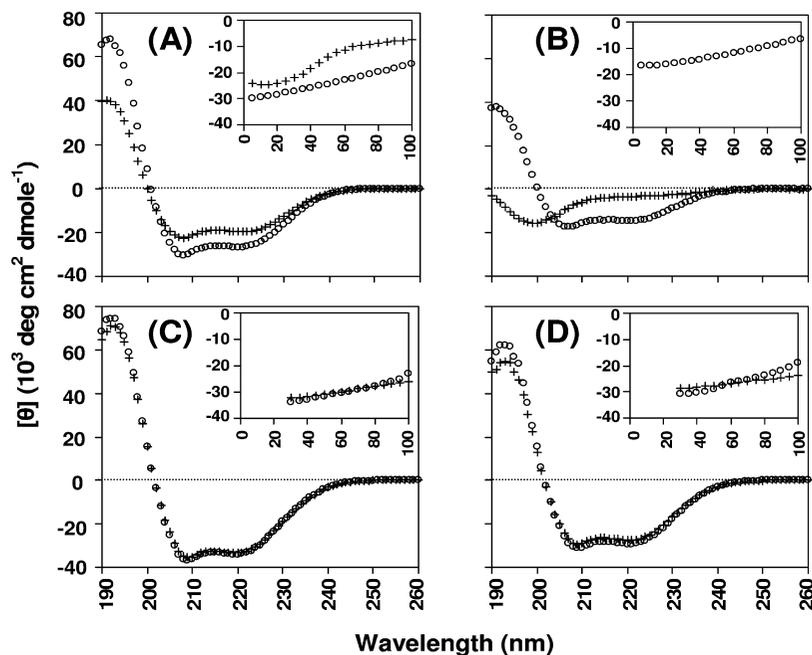
FIGURE 4: Far-UV CD analysis of gp41 constructs at 20 μM in either buffer (crosses) or detergent (open circles): (A) N70, (B) FP34, (C) N47(L6)C39, and (D) N70(L6)C39. Structured samples were heated to probe thermal stability (insets). For insets, the abscissa is the temperature scale in °C, and the ordinate is the mean residue molar ellipticity at 222 nm ($[\theta_{222}]$ (10^3 deg cm^2 dmol^{-1})).

Table 1: Relative α-Helicity of gp41 Constructs in Buffer and Detergent[a]

	% helicity in buffer	% helicity in detergent
FP34	10 (31)	44 (19)
N70	60 (28)	81 (14)
N47(L6)C39 "hairpin"	99 (1)	100 (0)
N70(L6)C39 "FP-hairpin"	82 (20)	88 (14)

[a] Data are based on molar ellipticity at 222 nm wavelength using −33000 deg cm^2 dmol^{-1} as 100% helicity. Estimated number of nonhelical residues in parentheses.

tide surface (*21, 23*). To reduce potential FP34 aggregation, FP34 was initially solubilized in detergent, and relative to solubilization in buffer, FP34 in detergent induces accelerated lipid mixing (Figure 3B). This acceleration correlates with an approximate 34% α-helical structure induction (Figure 4B and Table 1) and may be due to dissolution of aggregates.

The N47(L6)C39 construct adopts nearly 100% α-helical secondary structure in buffer and detergent (Figure 4C and Table 1) with high thermostability and no transition up to 100 °C (Figure 4C inset). These results are consistent with trimeric SHB structure stabilized by a leucine zipper formed from three molecules and correlate with earlier studies on closely related constructs, which include several high-resolution crystal structures (*12, 15, 24, 25*). Clore and co-workers showed that a similar construct which contains the native loop is strictly trimeric under the low pH conditions of 50 mM formate, pH 2.5 (*26*). Furthermore, trimeric hairpins were observed in the high-resolution structure of the N45(L6)C36 construct crystallized at neutral pH (*24*). This construct only differs from the N47(L6)C39 by truncation of two NHR residues and three CHR residues. Overall, these corollary data suggest that N47(L6)C39 is trimeric in buffer at pH 3.0 as well as physiologic pH. To further reduce the possibility of formation of aggregates of N47(L6)C39 trimers, comparative structure/function analyses were also carried out in detergent. The presence of D-malt does not affect the tertiary assembly of N47(L6)C39 based on the
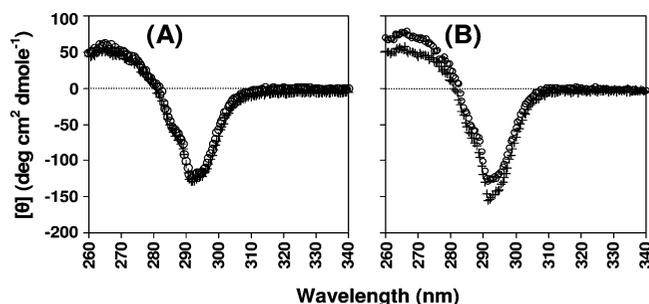

FIGURE 5: Near-UV CD analysis of gp41 constructs at 40 μM in either buffer (crosses) or detergent (open circles): (A) N47(L6)C39 and (B) N70(L6)C39.

similar aromatic dichroism signal in either buffer or detergent (Figure 5A), indicating that D-malt is nondenaturing. In some contrast, sodium dodecyl sulfate detergent at micellar concentrations ablates gp41 aromatic dichroism which is consistent with disruption of tertiary structure and monomeric protein organization. The latter conclusion correlates with gel electrophoresis data in sodium dodecyl sulfate (*27*). N47(L6)C39 is nonfusogenic (Figure 3A,B), and this result is independent of initial solubilization in buffer or detergent. This result is perhaps not surprising because N47(L6)C39 lacks the membrane-perturbing FP domain and highly thermostable gp41 hairpins do not disassemble in membranes (*28*). Given the ability of detergents to dissolve protein aggregates and the fact that N47(L6)C39 is well folded in detergent (Figure 5A), the fusion incompetence of N47(L6)C39 is likely not correlated with protein aggregation.

Approximately 20 residues are nonhelical for N70(L6)C39 in buffer, which differs from the fully helical N47(L6)C39 by inclusion of the N-terminal 23 residues (Figure 4C,D and Table 1). This is consistent with nonhelical FP residues in N70(L6)C39 as shown for hairpins formed by the free peptides N70 and C34 (*15*). N70(L6)C39 has a similar number of nonhelical residues in buffer as does N70, while in detergent both constructs have fewer nonhelical residues

(Figure 4A,D and Table 1). These data generally correlate with some fraction of nonhelical structure in the FP region of N70(L6)C39 in buffer and a smaller fraction in detergent (*15*). In both buffer and detergent N70(L6)C39 is highly helical (Figure 4D and Table 1) with high thermostability and no transition up to 100 °C (Figure 4D inset). These findings are qualitatively consistent with low-energy hairpin gp41 assembly, correlating with earlier studies on closely related constructs, which include several high-resolution crystal structures (*12, 15, 24, 25*). Hairpin structure is confirmed for an analogous complex comprised of the free peptides N70 and C34 (*15*). N70(L6)C39 was specifically designed to maintain covalent association between N- and C-helices by replacing the native loop with a minimal loop and includes a C-terminal five-residue extension in the C-helix region relative to the N70/C34 hairpin. These modifications are not expected to alter hairpin assembly but do significantly enhance thermal stability compared to the N70/C34 hairpin which melts with a transition temperature of 81 °C (*15*).

Because the FP region directs aggregation of N70/C34 hairpins in buffer (*15*), we expect a similar effect with N70(L6)C39, and therefore conducted comparative structure/function analyses in detergent to dissolve aggregates expected to be present in buffer. Near-UV CD analysis indicates that N70(L6)C39 is well folded in both detergent and buffer (Figure 5B). Despite apparent hairpin assembly, N70(L6)C39 is nonfusogenic (Figure 3A,B); i.e., inclusion of the FP does not increase lipid mixing beyond the basal level observed for N47(L6)C39. This is the result for initial N70(L6)C39 solubilization in either buffer or detergent, which indicates that FP-induced aggregation expected in buffer would not explain lack of fusion activity. Assuming N70(L6)C39 is well folded in low-energy hairpin conformation as the CD data qualitatively suggests, the most reasonable interpretation of the lipid mixing data is that the bulky charged hairpin domain interferes with the membrane-perturbing function of the FP domain.

We next tested fusion-defective N70(L6)C39 and N47(L6)C39 for their abilities to impede fusion directed by FP34. At 1:1.5 ratio of N70(L6)C39 to FP34 in buffer, lipid mixing by FP34 was effectively reduced by 9-fold due to N70(L6)C39 whether both constructs were initially premixed or added sequentially to vesicles (N70(L6)C39 followed by FP34, Figure 3C). Active lipid mixing by FP34 was arrested by addition of N70(L6)C39 at the same ratio (Figure 3C). For this experiment, a control was also done that was addition of an aliquot of pure buffer rather than N70(L6)C39 in buffer to the FP34/vesicle solution. As expected, this buffer aliquot did not affect lipid mixing induced by FP34 (data not shown). A second control was addition of an aliquot of FP34 in buffer to the FP34/vesicle solution. This added FP34 increased lipid mixing with the expected dose response (data not shown).

FP constructs coassemble in membranes (*21, 23, 29*). To test whether inhibition of FP34 is due to heteroassembly with the FP region of N70(L6)C39, the same experiments were carried out using N47(L6)C39 as the putative inhibitor. Very similar inhibitory effects were observed for N47(L6)C39 (data not shown). It is therefore unlikely that N70(L6)C39 inhibits FP34-induced fusion by direct FP interaction and suggests instead that the inhibition is due to the hairpin functionality. There are qualitatively similar effects when
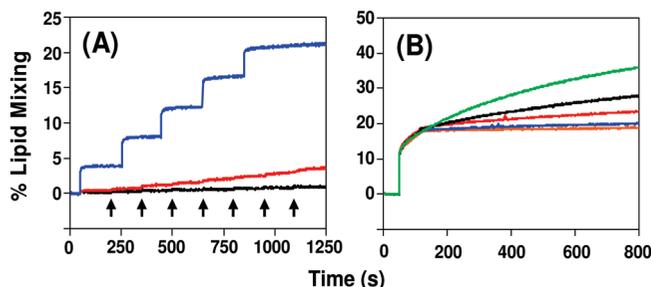

FIGURE 6: Lipid mixing of POPC:POPG:chol vesicles induced by gp41 constructs. At 50 s, an initial aliquot of protein or peptide was added to vesicles with 150 μM total lipid and 75 μM cholesterol concentrations. For panel A, aliquots of peptide or protein were added incrementally as follows: 0.5 μM aliquots added at 50 s and every 150 s thereafter, as indicated by arrows, of N70(L6)C39 initially in buffer (black) or detergent (red) and 0.2 μM aliquots added at 50 s and every 200 s thereafter up to 850 s of N70 in buffer (blue). For panel B, lipid mixing traces due to gp41 constructs in buffer are as follows: 2.0 μM FP34 (green), 2.0 μM FP34 with the addition at 120 s of N70(L6)C39 at 0.125 μM (black), 0.25 μM (red), 0.5 μM (blue), and 1.0 μM (orange).

FP34 and N70(L6)C39 are initially solubilized in detergent (Figure 3D) with 5-fold reduction in lipid mixing extent when the two proteins are premixed and 2-fold reduction when N70(L6)C39 is added first followed by FP34. Relative to solubilization in buffer, the reduced inhibitory effects of N70(L6)C39 with solubilization in detergent are likely due to the faster intrinsic fusion rate of FP34 in detergent (Figure 3A,B). Relative to FP34, there are smaller inhibitory effects on N70-induced lipid mixing by N47(L6)C39 and N70(L6)C39, which correlate with very rapid N70-induced mixing (data not shown).

Because N70(L6)C39 exhibits partial precipitation in pH 7.2 solution without vesicles, lipid mixing was also probed after addition of small soluble aliquots of N70(L6)C39 in either buffer or detergent to the vesicle solution (Figure 6A). Each aliquot increased the N70(L6)C39 concentration by 0.5 μM, which was comparable to the N70(L6)C39 solubility at pH 7.2 without vesicles. Negligible lipid mixing was observed after each addition and correlated with the negligible mixing observed for a single large aliquot of N70(L6)C39 (Figure 3A,B). The same experiment was done with N70 and served as a positive control indicating that very small amounts (0.2 μM) of fusion active N70 generate a rapid and consistent lipid-mixing dose response. These results indicate that the lack of fusogenicity of N70(L6)C39 is not correlated with protein precipitation. Interestingly, N70 at concentrations up to at least 3.3 μM has been shown to induce rapid lipid mixing in a dose-dependent manner for vesicles in pH 7.4 phosphate-buffered saline solution (*16*) despite observation of minimal solubility of N70 (<0.2 μM) in pH 7.4 phosphate-buffered saline without vesicles (measured in the present study). Additional experiments were done to test the dose response of inhibition of FP34-induced lipid mixing by N70(L6)C39 (Figure 6B). Inhibition was clearly augmented with larger aliquots of N70(L6)C39 and was not obviously correlated with any increased precipitation at higher concentrations of N70(L6)C39.

Fusion protein interaction with vesicles may lead to larger vesicular bodies because of either vesicle fusion or vesicle aggregation without fusion (*16*). These larger bodies will scatter visible light to a greater extent than the initial vesicles.

Under the conditions of the lipid mixing assay, both N70 and FP34 induced an increase in vesicle particle size as evidenced by larger absorbance at 405 nm in samples with protein and vesicles relative to samples with vesicles alone. In some contrast, incubation of the vesicles with N47(L6)C39 initially in buffer or detergent resulted in an absorbance at 405 nm which, within experimental error, was the same as that observed with vesicles alone. N47(L6)C39 therefore induces neither aggregation of vesicles nor lipid mixing between these vesicles.

DISCUSSION

The key findings of the present work are as follows: (a) the minimal "FP-hairpin" N70(L6)C39 construct does not induce significant vesicle fusion; (b) both N70(L6)C39 and the "hairpin" N47(L6)C39 construct inhibit vesicle fusion induced by FP34 or N70; and (c) N70 trimers, which model exposed N-PHI organization (15), induce rapid and extensive vesicle fusion. To accurately quantify the rapid lipid mixing rate of N70 in buffer and detergent, further studies on the millisecond time scale would be needed. The lack of activity of N70(L6)C39 was initially surprising because the protein appears to have stable hairpin structure and therefore trimeric FP topology. This topology has been associated with rapid vesicle fusion induced by chemically cross-linked FP trimers (17), and the present results show that trimerization of the FP by the NHR coiled coil in N70 (15) is also correlated with extremely rapid vesicle fusion. The lack of fusion activity of N70(L6)C39 indicates that trimeric FP topology is not sufficient for fusion induction and that the fusogenic enhancement correlated with this topology can be counteracted by the hairpin region.

Although assembly of FPs from different molecules has been observed for membrane-associated FP34 and for membrane-associated N70 (29), inhibition of FP34 lipid mixing by N70(L6)C39 is not due to heteroassembly of the apolar FP regions of both molecules. Similar inhibition of FP34-induced fusion by both N47(L6)C39 and N70(L6)C39 suggests instead that the hairpin region rather than the FP region is the source of inhibition. In addition, inhibition is observed when either N70(L6)C39 or N47(L6)C39 is first added to the vesicle solution followed by FP34. This suggests that the hairpin region interacts with the vesicles in a manner which reduces the membrane-perturbing effect of the FP. While membrane binding by folded gp41 constructs containing the native loop and lacking the FP has been shown for HIV (30), and for well-defined SIV hairpin trimers (28), the mechanism of fusion inhibition by hairpins is not clear and warrants further investigation.

The partial precipitation of N70(L6)C39 in pH 7.2 solutions without vesicles was not obviously correlated with the fusion properties of this construct. Negligible fusion was induced either after addition of small soluble aliquots or after addition of a single large aliquot. In addition, fusion inhibition by N70(L6)C39 showed a clear dose response, and similar inhibition was observed for both N70(L6)C39 and N47(L6)C39 with respective low and high solubilities at pH 7.2. Studies have also shown that vesicle fusion was induced by N70 and a 23-mer FP fragment even when these constructs were poorly soluble in the absence of vesicles (16, 31).

The lack of activity of N70(L6)C39 is in stark contrast to the rapid vesicle fusion induced by N70 and may have

biological relevance. In particular, during HIV/host cell fusion, the PHI gp41 conformation is formed prior to the hairpin conformation, and the hairpin is considered to be the final gp41 ectodomain structure during fusion (1, 2). Cell−cell fusion experiments between cells expressing HIV ENV and those expressing CD4 and coreceptor indicate that gp41 exists in an exposed conformation (PHI) through the hemifusion (lipid mixing) and initial fusion pore formation (contents mixing) steps (10). Although complete folding into hairpins occurs after initial pore formation, hairpins have been shown to play a role in fusion pore stabilization (10). The lipid mixing assay of the present study is more closely aligned with hemifusion than with fusion pore formation so the rapid lipid mixing induced by the N-PHI construct, N70, and inhibition of lipid mixing by the hairpin constructs, N47(L6)C39 and N70(L6)C39, generally correlate with the cell−cell fusion results. Other data which correlate with these results are observations of vesicle fusion induced by a gp41 construct corresponding to the C-PHI or C-terminal half of the PHI (32) (see Figure 1B) and membrane pore formation induced by N70 (33). We qualify our hypothesis that final hairpin structure (represented by N70(L6)C39 and N47(L6)C39) arrests viral fusion with the caveat that both ectodomain constructs lack the C-terminal MPER region which is important in fusion (34−36) as well as the native loop region which may be involved in gp41 fusion (37). Despite this caveat, our interpretation is supported by an earlier observation that constructs similar to N47(L6)C39 with stable hairpin structure inhibit cell−cell fusion (38). Fusion inhibition by the final hairpin structure is also consistent with the reasonable view that host cell viability after completing the fusion process depends on arresting the plasma membrane perturbation induced by the FP.

These results on N70(L6)C39 are in some contrast to the rapid vesicle and cell−cell hemifusion at pH 5 induced by influenza virus fusion protein ectodomain constructs (39−41). The low pH requirement correlates with endocytosis of the influenza virus and fusion occurring inside the endosome. Although structures of fragments of the ectodomains of the HIV and influenza virus fusion proteins both show a long trimeric NHR region, the influenza protein lacks a long CHR region (2, 24, 42). The influenza virus ectodomain-induced vesicle fusion might therefore be more analogous with N70 which has an exposed NHR region than with N70(L6)C39 for which much of the NHR is covered by the CHR.

In conclusion, we find that trimeric FP assembly in context of N70 induces rapid and extensive vesicle fusion, which correlates with the ability of the PHI of gp41 to direct processes of membrane fusion through the stage of pore formation (10). The highly stable hairpin conformation abrogates the fusogenic capability of trimeric FP appendages, and nonfusogenic hairpin constructs interfere with the fusogenic function of FP and N-PHI constructs. These latter two findings correlate with a viral fusion role for folded hairpins that involves stabilization of fused bilayer structure (10).

the plate reader. The Mass Spectroscopy Facility at Michigan State University was used to carry out this research.

REFERENCES

1. Chan, D. C., and Kim, P. S. (1998) HIV entry and its inhibition. *Cell 93*, 681–684.

2. Weissenhorn, W., Dessen, A., Harrison, S. C., Skehel, J. J., and Wiley, D. C. (1997) Atomic structure of the ectodomain from HIV-1 gp41. *Nature 387*, 426–430.

3. Center, R. J., Leapman, R. D., Lebowitz, J., Arthur, L. O., Earl, P. L., and Moss, B. (2002) Oligomeric structure of the human immunodeficiency virus type 1 envelope protein on the virion surface. *J. Virol. 76*, 7863–7867.

4. Dalgleish, A. G., Beverley, P. C., Clapham, P. R., Crawford, D. H., Greaves, M. F., and Weiss, R. A. (1984) The CD4 (T4) antigen is an essential component of the receptor for the AIDS retrovirus. *Nature 312*, 763–767.

5. Feng, Y., Broder, C. C., Kennedy, P. E., and Berger, E. A. (1996) HIV-1 entry cofactor: functional cDNA cloning of a seven-transmembrane, G protein-coupled receptor. *Science 272*, 872–877.

6. Furuta, R. A., Wild, C. T., Weng, Y., and Weiss, C. D. (1998) Capture of an early fusion-active conformation of HIV-1 gp41. *Nat. Struct. Biol. 5*, 276–279.

7. Jones, P. L., Korte, T., and Blumenthal, R. (1998) Conformational changes in cell surface HIV-1 envelope glycoproteins are triggered by cooperation between cell surface CD4 and co-receptors. *J. Biol. Chem. 273*, 404–409.

8. Durell, S. R., Martin, I., Ruysschaert, J. M., Shai, Y., and Blumenthal, R. (1997) What studies of fusion peptides tell us about viral envelope glycoprotein-mediated membrane fusion (review). *Mol. Membr. Biol. 14*, 97–112.

9. White, J. M. (1992) Membrane fusion. *Science 258*, 917–924.

10. Markosyan, R. M., Cohen, F. S., and Melikyan, G. B. (2003) HIV-1 envelope proteins complete their folding into six-helix bundles immediately after fusion pore formation. *Mol. Biol. Cell 14*, 926–938.

11. Chan, D. C., Fass, D., Berger, J. M., and Kim, P. S. (1997) Core structure of gp41 from the HIV envelope glycoprotein. *Cell 89*, 263–273.

12. Tan, K., Liu, J., Wang, J., Shen, S., and Lu, M. (1997) Atomic structure of a thermostable subdomain of HIV-1 gp41. *Proc. Natl. Acad. Sci. U.S.A. 94*, 12303–12308.

13. Freed, E. O., Delwart, E. L., Buchschacher, G. L., Jr., and Panganiban, A. T. (1992) A mutation in the human immunodeficiency virus type 1 transmembrane glycoprotein gp41 dominantly interferes with fusion and infectivity. *Proc. Natl. Acad. Sci. U.S.A. 89*, 70–74.

14. Kilby, J. M., Hopkins, S., Venetta, T. M., DiMassimo, B., Cloud, G. A., Lee, J. Y., Alldredge, L., Hunter, E., Lambert, D., Bolognesi, D., Matthews, T., Johnson, M. R., Nowak, M. A., Shaw, G. M., and Saag, M. S. (1998) Potent suppression of HIV-1 replication in humans by T-20, a peptide inhibitor of gp41-mediated virus entry. *Nat. Med. 4*, 1302–1307.

15. Sackett, K., Wexler-Cohen, Y., and Shai, Y. (2006) Characterization of the HIV N-terminal fusion peptide-containing region in context of key gp41 fusion conformations. *J. Biol. Chem. 281*, 21755–21762.

16. Sackett, K., and Shai, Y. (2002) The HIV-1 gp41 N-terminal heptad repeat plays an essential role in membrane fusion. *Biochemistry 41*, 4678–4685.

17. Yang, R., Prorok, M., Castellino, F. J., and Weliky, D. P. (2004) A trimeric HIV-1 fusion peptide construct which does not self-associate in aqueous solution and which has 15-fold higher membrane fusion rate. *J. Am. Chem. Soc. 126*, 14722–14723.

18. Brugger, B., Glass, B., Haberkant, P., Leibrecht, I., Wieland, F. T., and Krausslich, H. G. (2006) The HIV lipidome: a raft with an unusual composition. *Proc. Natl. Acad. Sci. U.S.A. 103*, 2641–2646.

19. Struck, D. K., Hoekstra, D., and Pagano, R. E. (1981) Use of resonance energy transfer to monitor membrane fusion. *Biochemistry 20*, 4093–4099.

20. Yang, J., Gabrys, C. M., and Weliky, D. P. (2001) Solid-state nuclear magnetic resonance evidence for an extended beta strand conformation of the membrane-bound HIV-1 fusion peptide. *Biochemistry 40*, 8126–8137.

21. Yang, J., Prorok, M., Castellino, F. J., and Weliky, D. P. (2004) Oligomeric beta-structure of the membrane-bound HIV-1 fusion peptide formed from soluble monomers. *Biophys. J. 87*, 1951–1963.

22. Jaroniec, C. P., Kaufman, J. D., Stahl, S. J., Viard, M., Blumenthal, R., Wingfield, P. T., and Bax, A. (2005) Structure and dynamics of micelle-associated human immunodeficiency virus gp41 fusion domain. *Biochemistry 44*, 16167–16180.

23. Kliger, Y., Aharoni, A., Rapaport, D., Jones, P., Blumenthal, R., and Shai, Y. (1997) Fusion peptides derived from the HIV type 1 glycoprotein 41 associate within phospholipid membranes and inhibit cell-cell fusion. Structure-function study. *J. Biol. Chem. 272*, 13496–13505.

24. Bai, X., Wilson, K. L., Seedorff, J. E., Ahrens, D., Green, J., Davison, D. K., Jin, L., Stanfield-Oakley, S. A., Mosier, S. M., Melby, T. E., Cammack, N., Wang, Z., Greenberg, M. L., and Dwyer, J. J. (2008) Impact of the enfuvirtide resistance mutation N43D and the associated baseline polymorphism E137K on peptide sensitivity and six-helix bundle structure. *Biochemistry 47*, 6662–6670.

25. Shu, W., Ji, H., and Lu, M. (2000) Interactions between HIV-1 gp41 core and detergents and their implications for membrane fusion. *J. Biol. Chem. 275*, 1839–1845.

26. Caffrey, M., Braddock, D. T., Louis, J. M., Abu-Asab, M. A., Kingma, D., Liotta, L., Tsokos, M., Tresser, N., Pannell, L. K., Watts, N., Steven, A. C., Simon, M. N., Stahl, S. J., Wingfield, P. T., and Clore, G. M. (2000) Biophysical characterization of gp41 aggregates suggests a model for the molecular mechanism of HIV-associated neurological damage and dementia. *J. Biol. Chem. 275*, 19877–19882.

27. Lin, C. H., Chang, C. C., Cheng, S. F., and Chang, D. K. (2008) The application of perfluorooctanoate to investigate trimerization of the human immunodeficiency virus-1 gp41 ectodomain by electrophoresis. *Electrophoresis 29*, 3175–3182.

28. Peisajovich, S. G., Blank, L., Epand, R. F., Epand, R. M., and Shai, Y. (2003) On the interaction between gp41 and membranes: the immunodominant loop stabilizes gp41 helical hairpin conformation. *J. Mol. Biol. 326*, 1489–1501.

29. Sackett, K., and Shai, Y. (2005) The HIV fusion peptide adopts intermolecular parallel beta-sheet structure in membranes when stabilized by the adjacent N-terminal heptad repeat: a ^{13}C FTIR study. *J. Mol. Biol. 350*, 790–805.

30. Kliger, Y., Peisajovich, S. G., Blumenthal, R., and Shai, Y. (2000) Membrane-induced conformational change during the activation of HIV-1 gp41. *J. Mol. Biol. 301*, 905–914.

31. Pereira, F. B., Goni, F. M., Muga, A., and Nieva, J. L. (1997) Permeabilization and fusion of uncharged lipid vesicles induced by the HIV-1 fusion peptide adopting an extended conformation: dose and sequence effects. *Biophys. J. 73*, 1977–1986.

32. Shnaper, S., Sackett, K., Gallo, S. A., Blumenthal, R., and Shai, Y. (2004) The C- and the N-terminal regions of glycoprotein 41 ectodomain fuse membranes enriched and not enriched with cholesterol, respectively. *J. Biol. Chem. 279*, 18526–18534.

33. Korazim, O., Sackett, K., and Shai, Y. (2006) Functional and structural characterization of HIV-1 gp41 ectodomain regions in phospholipid membranes suggests that the fusion-active conformation is extended. *J. Mol. Biol. 364*, 1103–1117.

34. Lorizate, M., Huarte, N., Saez-Cirion, A., and Nieva, J. L. (2008) Interfacial pre-transmembrane domains in viral proteins promoting membrane fusion and fission. *Biochim. Biophys. Acta 1778*, 1624–1639.

35. Salzwedel, K., West, J. T., and Hunter, E. (1999) A conserved tryptophan-rich motif in the membrane-proximal region of the human immunodeficiency virus type 1 gp41 ectodomain is important for Env-mediated fusion and virus infectivity. *J. Virol. 73*, 2469–2480.

36. Suarez, T., Nir, S., Goni, F. M., Saez-Cirion, A., and Nieva, J. L. (2000) The pre-transmembrane region of the human immunodeficiency virus type-1 glycoprotein: a novel fusogenic sequence. *FEBS Lett. 477*, 145–149.

37. Pascual, R., Moreno, M. R., and Villalain, J. (2005) A peptide pertaining to the loop segment of human immunodeficiency virus gp41 binds and interacts with model biomembranes: implications for the fusion mechanism. *J. Virol. 79*, 5142–5152.

38. Lu, M., Ji, H., and Shen, S. (1999) Subdomain folding and biological activity of the core structure from human immunodeficiency virus type 1 gp41: implications for viral membrane fusion. *J. Virol. 73*, 4433–4438.

39. Curtis-Fisk, J., Preston, C., Zheng, Z. X., Worden, R. M., and Weliky, D. P. (2007) Solid-state NMR structural measurements on the membrane-associated influenza fusion protein ectodomain. *J. Am. Chem. Soc. 129*, 11320–11321.

40. Epand, R. F., Macosko, J. C., Russell, C. J., Shin, Y. K., and Epand, R. M. (1999) The ectodomain of HA2 of influenza virus promotes rapid pH dependent membrane fusion. *J. Mol. Biol. 286*, 489–503.

41. Leikina, E., LeDuc, D. L., Macosko, J. C., Epand, R., Epand, R., Shin, Y. K., and Chernomordik, L. V. (2001) The 1−127 HA2 construct of influenza virus hemagglutinin induces cell-cell hemi-fusion. *Biochemistry 40*, 8378–8386.

42. Chen, J., Skehel, J. J., and Wiley, D. C. (1999) N- and C-terminal residues combine in the fusion-pH influenza hemagglutinin HA(2) subunit to form an N cap that terminates the triple-stranded coiled coil. *Proc. Natl. Acad. Sci. U.S.A. 96*, 8967–8972.